



Structure and stability of binary transition-metal clusters $(\text{NbCo})_n$ ($n \leq 5$): A relativistic density-functional study

Xian Wang, Zexing Cao, Xin Lu, Menghai Lin, and Qianer Zhang

Citation: *J. Chem. Phys.* **123**, 064315 (2005); doi: 10.1063/1.1999634

View online: <http://dx.doi.org/10.1063/1.1999634>

View Table of Contents: <http://jcp.aip.org/resource/1/JCPSA6/v123/i6>

Published by the [American Institute of Physics](http://www.aip.org).

Related Articles

Electron interaction with nitromethane embedded in helium droplets: Attachment and ionization measurements
J. Chem. Phys. **135**, 174504 (2011)

Geometry optimization of bimetallic clusters using an efficient heuristic method
J. Chem. Phys. **135**, 164109 (2011)

Solvation effects on angular distributions in $\text{H}(\text{NH}_3)_n$ and $\text{NH}_2(\text{NH}_3)_n$ photodetachment: Role of solute electronic structure
J. Chem. Phys. **135**, 164301 (2011)

A fast variational Gaussian wavepacket method: Size-induced structural transitions in large neon clusters
J. Chem. Phys. **135**, 154106 (2011)

Raman spectroscopy and microscopy based on mechanical force detection
Appl. Phys. Lett. **99**, 161103 (2011)

Additional information on *J. Chem. Phys.*

Journal Homepage: <http://jcp.aip.org/>

Journal Information: http://jcp.aip.org/about/about_the_journal

Top downloads: http://jcp.aip.org/features/most_downloaded

Information for Authors: <http://jcp.aip.org/authors>

ADVERTISEMENT



AIP Advances

Submit Now

Explore AIP's new
open-access journal

- Article-level metrics now available
- Join the conversation! Rate & comment on articles

Structure and stability of binary transition-metal clusters $(\text{NbCo})_n$ ($n \leq 5$): A relativistic density-functional study

Xian Wang, Zexing Cao,^{a)} Xin Lu, Menghai Lin,^{b)} and Qianer Zhang
*Department of Chemistry, State Key Laboratory of Physical Chemistry of Solid Surfaces,
and Center for Theoretical Chemistry, Xiamen University, Xiamen 361005, China*

(Received 16 May 2005; accepted 14 June 2005; published online 17 August 2005)

Equilibrium geometries and electronic properties of binary transition-metal clusters, $(\text{NbCo})_n$ ($n \leq 5$), have been investigated by means of the relativistic density-functional approach. The metal-metal bonding and stability aspects of these clusters have been analyzed on the basis of calculations. Present results show that these clusters exhibit rich structural varieties on the potential-energy surfaces. The most stable structures have a compact conformation in relatively high symmetry, in which the Nb atoms prefer to form an inner core and Co atoms are capped to the facets of the core. Such building features in clustering of the Nb/Co system are related to the order of bond strength: $\text{Nb-Nb} > \text{Nb-Co} > \text{Co-Co}$. As the binary cluster size increases, the Nb-Co bond may become stronger than the Nb-Nb bond in the inner niobium core, which results in a remarkable increment of the Nb-Nb bond length. Amongst these binary transition-metal clusters, the singlet $(\text{NbCo})_4$ in T_d symmetry has a striking high stability due to the presence of the spherical aromaticity and electronic shell closure. The size dependence of the bond length and stability of the cluster has been explored. © 2005 American Institute of Physics. [DOI: 10.1063/1.1999634]

I. INTRODUCTION

Transition-metal (TM) clusters as a type of unusual chemical entity have received considerable attention both experimentally and theoretically.¹⁻⁴ While earlier investigations on TM clusters focused on monometallic clusters, binary TM alloy clusters and multicomponent metal clusters have become a subject of recent experimental and theoretical studies due to their potential applications in materials and catalysis.⁵⁻⁹

The bimetallic Co/M ($M = \text{V}, \text{Al}, \text{Rh}$) systems, as a typical series of binary TM clusters, have been extensively studied by various experimental techniques and theoretical calculations.¹⁰⁻¹⁶ Previous studies have revealed a notable effect of the inhomogeneity of bimetallic clusters on their physical and chemical properties. For example, Hoshino *et al.* studied ionization energies of cobalt-vanadium bimetallic clusters (Co_nV_m) and their reactivity toward H_2 .¹¹ Their studies show that the local charge density and the geometric structure play an important role in determining chemisorption reactivity. Bulk $4d$ metals such as Rh are generally non-magnetic, while the substitution of Rh by Co atoms gives rise to a significant increase of the local magnetic moment at the Rh neighbors.^{14,16} Recent studies on magnetism of the well-defined cobalt clusters embedded in a niobium matrix indicate that there is a “magnetically dead” Co/Nb alloy interface.^{17,18} Computational modeling suggests that the number of Nb atoms in the nearest neighbor of the Co atom

is crucial for the formation of the magnetically dead layer. If the number is greater than 5, the Co magnetic moment basically vanishes.¹⁹

Homonuclear niobium²⁰⁻²² and cobalt²³⁻²⁵ clusters have been extensively studied. Generally, the niobium clusters have compact structures with low spin states due to strong metal-metal bonding interactions, while the cobalt clusters exist in high spin states with large magnetic moments. These transition-metal clusters in high symmetry usually suffer Jahn-Teller (JT) distortion. For example, Nb_3 in D_{3h} symmetry is unstable and the JT effect arising from nearly isoenergetic a'_1 and e'' orbitals results in a stable C_{2v} structure.²¹ Similar JT distortions also exist in cobalt clusters.^{24,25} Co and Nb approximately complement each other in their valence electrons. At present, the cooperative effect in the Nb/Co system on their electronic and magnetic properties is still unclear. In our previous study,²⁶ a detailed comparison among Nb_4 , Co_4 , and $(\text{NbCo})_2$ was carried out on the basis of nonrelativistic density-functional theory (DFT) calculations. Theoretical results indicate that the heterometallic cluster Nb_2Co_2 has a complicated metal-metal bonding, which leads to a rich structural variety.

In the present study, we have carried out a systematic research of $(\text{NbCo})_n$ ($n \leq 5$) clusters by the relativistic density-functional approach. The structural and electronic properties of the clusters as well as their general trends as the cluster size increases have been discussed.

II. COMPUTATIONAL DETAILS

DFT calculations were performed for the various electronic states of these metal clusters with the Amsterdam density functional (ADF) package.²⁷ The molecular orbitals (MOs) were expanded in an uncontracted set of Slater-type

^{a)}Electronic mail: zxcao@xmu.edu.cn

^{b)}Author to whom correspondence should be addressed. Fax: +86-592-2183047. Electronic mail: linmh@xmu.edu.cn

TABLE I. Bond lengths (R_e in Å), vibrational frequency (ω_e in cm^{-1}), and the dissociation energy (D_0^o in eV) for the ground state of Nb_2 and Co_2 .

	Method	State	R_e	ω_e	D_0^o
Nb_2	PW91	$^3\Sigma_g^-$	2.08	456.7	4.87
	LSDA	$^3\Sigma_g^-$	2.12 ^a	451.05 ^a	5.03 ^a
	LDA	$^3\Sigma_g^-$	2.08 ^b	472 ^b	5.8 ^b
	GGA	$^3\Sigma_g^-$	2.10 ^b	447 ^b	5.4 ^b
	Expt.	$^3\Sigma_g^-$	2.078 ^c	424.8917 ^c	5.19±0.28 ^d and 5.48 ^e
Co_2	PW91	$^5\Delta_g$	2.02	384.9	1.82
	GGA	$^5\Delta_g$	2.01 ^f	342 ^f	2.26 ^f
	BP86		2.04 ^g		2.85 ^g
	Expt.			296.8±0.54 ^h	1.69±0.26 ⁱ
NbCo	PW91	$^3\Delta$	2.02	310.4	3.08
	Expt.	$^3\Delta$			2.729±0.001 ^j

^aReference 34.^bReference 35.^cReference 31.^dReference 32.^eReference 33.^fReference 25.^gReference 36.^hReference 38.ⁱReference 37.^jReference 39.

orbitals (STOs) containing diffuse functions. The Perdew-Wang 91 (PW91) (Ref. 28) generalized gradient approximation of the exchange-correlation functional was used throughout in the calculation. In consideration of the relativistic effects of these transition metals, a combined scalar relativistic zero-order regular approximation^{29,30} (ZORA) has been taken into account and a frozen-core triple- ζ basis set plus double polarization functions has been used for these cases. The inner shells of niobium and cobalt atoms are kept frozen up to 3*d* and 2*p* orbitals, respectively. Analytical frequency calculations were performed for all stationary points located on the potential-energy surfaces (PESs) to assess the nature of an optimized structure. In determination of the most stable structures of mixed clusters, various initial geometries with different spin states in possible symmetries are considered.

To validate the reliability of the present calculation, related dimers Nb_2 , Co_2 , and NbCo have been calculated as a

test. Table I presents equilibrium bond lengths, vibrational frequencies, and dissociation energies of such dimers. The present PW91 results of Nb_2 in Table I show a good agreement with previous experimental^{31–33} and theoretical^{34,35} values. For Co_2 , the PW91 bond length agrees with the reported theoretical results,^{25,36} and its dissociation energy of 1.82 eV may match the experimental value of 1.69±0.26 eV.³⁷ In the case of NbCo , the present dissociation energy is 3.08 eV, slightly higher than the experimental value of 2.729±0.001 eV.³⁹

III. RESULTS AND DISCUSSION

The optimized structures and relative energies of the binary clusters $(\text{NbCo})_n$ ($2 \leq n \leq 5$) at various spin states are displayed in Figs. 1–4, where the dark circle and empty circle

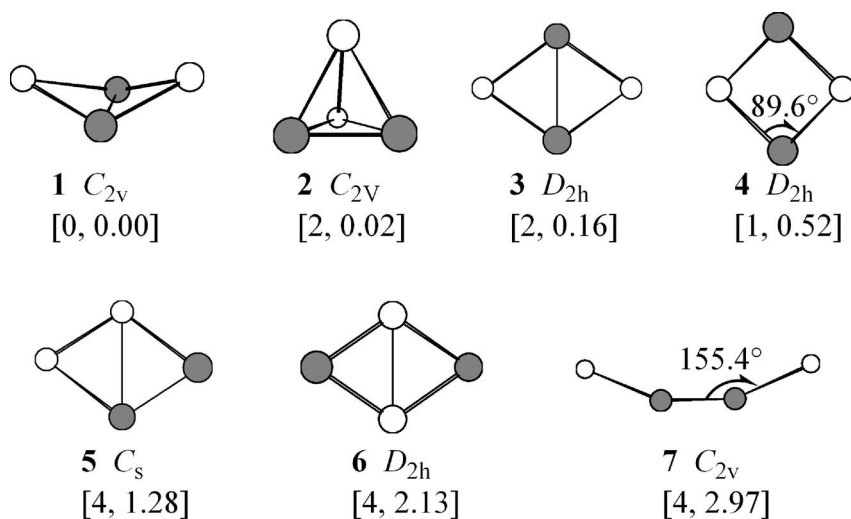


FIG. 1. Optimized geometries of $(\text{NbCo})_2$ clusters are shown with their spin (S) and relative energies (ΔE in eV), $[S, \Delta E]$, where the dark circle and empty circle correspond to Nb and Co atoms, respectively.

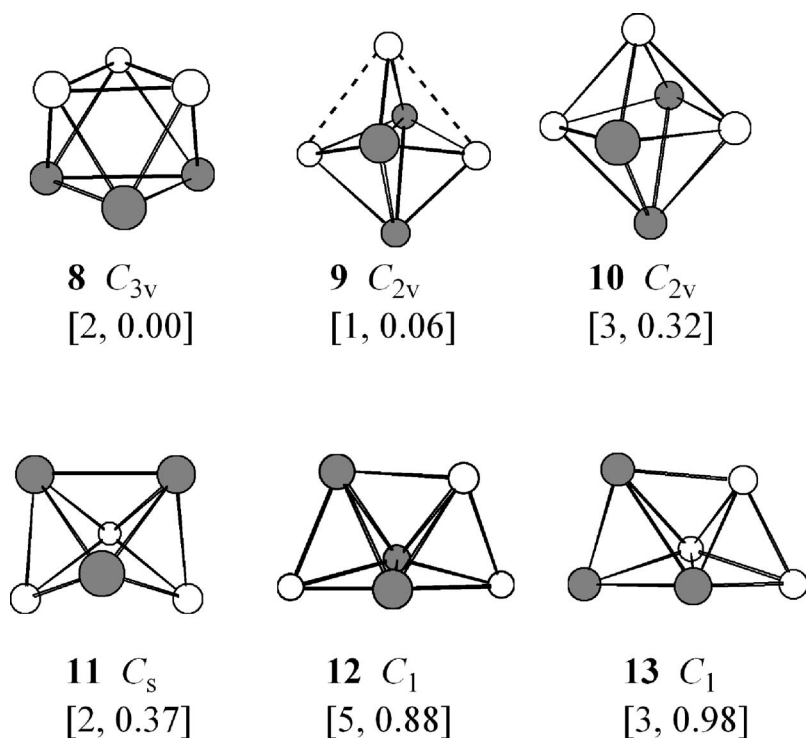


FIG. 2. Optimized geometries of $(\text{NbCo})_3$ clusters are shown with their spin (S) and relative energies (ΔE in eV), $[S, \Delta E]$, where the dark circle and empty circle correspond to Nb and Co atoms, respectively.

circle correspond to Nb and Co atoms, respectively. Optimized bond lengths of different topological structures with the lower energy are collected in Table II.

A. Structures

1. $(\text{NbCo})_2$

The equilibrium geometries and relative energies of $(\text{NbCo})_2$ isomers are displayed in Fig. 1. As Fig. 1 shows, the three-dimensional (3D) structure is slightly more stable than the planar and linear forms. Our previous DFT calculations²⁶ at the nonrelativistic level of theory found the most stable isomer to have a tetrahedral structure. Present scalar relativistic treatments predict that the tetrahedral isomers ($S=2$ and 3) have strong Nb–Nb bonds and weak Co–Co bonds and they are slightly less stable than open butterfly-shaped structures ($S=0$ and 1), in which the most stable species (1) with a dihedral angle of 138.5° has a closed-shell electronic structure. Since the butterfly-shaped 1 in the 1A_1 state and the tetrahedral 2 in the 5A_1 state have a small energy splitting of 0.02 eV, they are considered as isoenergetic isomers. The planar isomers (3–6) with various electronic spin states ($S=1$ –4) are higher in energy than the most stable structure 1 by about 0.16–2.13 eV. The binary metallic chain 7 is the highest one in energy amongst the stable isomers of $(\text{NbCo})_2$ in Fig. 1 due to the inclusion of less metal-metal bonds.

2. $(\text{NbCo})_3$

For the $(\text{NbCo})_3$ cluster, only 3D structures are found to be stable though the one-, two-, and three-dimensional initial structures have been considered in optimization. Figure 2 displays the stable structures. The most stable isomer 8 has a staggered trigonal prism in C_{3v} symmetry. Its singly highest occupied orbitals are $(a_2)^1(e)^2(a_1)^1$. The a_2 orbital arises purely from $3d$ orbitals of the Co atoms, whereas a_1 and

degenerate e orbitals have an obvious character of bonding molecular orbitals from Nb and Co. In this species, the net spin populations at Co and Nb are 1.38 and -0.05 , respectively, indicating that most of the electrons of Nb are coupled for the metal-metal bonding. Bond lengths of Nb–Nb, Co–Nb, and Co–Co bonds are 2.56, 2.36, and 2.34 Å, respectively, and their corresponding Mulliken bonding populations are 0.76, 0.55, and 0.32. The Nb–Nb bond is thus the strongest and the next one is the Nb–Co bond. This is consistent with the dissociation energies of dimers in Table I. A similar structure in singlet state ($^1A'$) is higher in energy than 8 by 0.34 eV.

The next stable isomer is a distorted octahedron 9 in the 3B_2 state, which is slightly less stable than 8 by 0.06 eV. Distortion of 9 by shortening the Co–Co bonds and expanding the center Nb–Nb bond leads to an octahedral isomer 10, which is 0.32 eV above 8. Other three isomers (11–13) with low or without symmetry were found to be less stable than 8 by 0.37–0.98 eV.

3. $(\text{NbCo})_4$

Optimized geometries of the $(\text{NbCo})_4$ cluster have been displayed in Fig. 3. The lowest-energy species 14 has a structure in T_d symmetry, in which Nb_4 forms a tetrahedral core and Co atoms are capped to the triangular facets of the Nb_4 core. Predicted Nb–Nb and Nb–Co bond distances in 14 are 2.84 and 2.32 Å, respectively. The structure 14 in a closed-shell 1A_1 state is much more stable than other tautomers. Such high stability of 14 in the 1A_1 state can be ascribed into the metallic aromaticity (*vide infra*). Other higher spin states ($S=1$ –5) with the same geometry as 14 are found to be stable by the PW91 calculation, but they are slightly higher in energy than the singlet state.

TABLE II. Energy gaps of HOMO and LUMO ($E_{\text{H-L}}$ in eV), binding energy per atom (E_b in eV), average Mulliken charges (\bar{Q}), average atom spin densities ($\bar{\rho}$), and average bond lengths (\bar{R} in Å) of the low-lying states $(\text{NbCo})_n$ ($2 \leq n \leq 5$). The corresponding Mulliken overlap populations (MOPs) are displayed in parentheses.

n	No.	$E_{\text{H-L}}$	E_b	\bar{Q}		$\bar{\rho}$		\bar{R} (MOP)		
				Nb	Co	Nb	Co	Nb–Nb	Nb–Co	Co–Co
2	1	0.48	2.78	0.15	−0.15	0	0	2.26(1.11)	2.29(0.67)	
	2	0.34	2.77	0.03	−0.03	0.39	1.61	2.28(1.20)	2.35(0.53)	2.50(0.16)
	3	0.42	2.74	0.10	−0.10	1.05	0.95	2.57(0.63)	2.22(0.80)	
3	7	0.27	2.03	0.04	−0.04	−0.11	2.08	2.13(1.42)	2.35(0.88)	
	8	0.53	3.68	0.04	−0.04	−0.05	1.38	2.56(0.76)	2.36(0.55)	2.34(0.32)
	9	0.36	3.60	0.04	−0.04	0.31	0.35	2.72(0.46)	2.33(0.58)	2.87(0.09)
	10	0.44	3.55	0.01	−0.01	0.52	1.48	2.55(0.61)	2.39(0.49)	2.50(0.29)
4	11	0.29	3.55	0.03	−0.03	−0.06	1.40	2.56(0.70)	2.37(0.56)	2.26(0.39)
	14	0.49	4.05	0.12	−0.12	0	0	2.84(0.40)	2.32(0.55)	
	17	0.28	3.96	0.08	−0.08	0.14	0.86	2.80(0.44)	2.37(0.49)	2.42(0.29)
	18	0.24	3.82	0.09	−0.09	0	0	2.65(0.57)	2.43(0.44)	2.34(0.34)
5	19	0.06	3.86	0.12	−0.12	0.25	1.25	2.60(0.42)	2.41(0.47)	2.30(0.23)
	22	0.18	3.78	0.07	−0.07	0.36	0.14	2.88(0.30)	2.36(0.50)	2.56(0.22)
	25	0.24	3.95	0.16	−0.16	0.32	0.88	2.90(0.24)	2.37(0.54)	
	28	0.29	3.80	0.09	−0.09	0.04	0.76	2.78(0.42)	2.39(0.41)	2.49(0.28)
	30	0.29	3.88	0.13	−0.13	0.25	0.97	2.82(0.25)	2.40(0.52)	2.36(0.24)
	35	0.32	3.88	0.07	−0.07	0.09	1.51	2.71(0.33)	2.47(0.39)	2.37(0.33)

The stability of the capped tetrahedron is sensitive to the arrangement of niobium and cobalt atoms in $(\text{NbCo})_4$. For instance, transpositions of Nb and Co in 14 result in isomers 15 and 16, which are less stable than 14 by 1.68 and 2.58 eV. Such instability of 15 and 16 arises from the decrease of

strong Nb–Nb bonds and increase of weak Co–Co bonds. A monocapped pentagonal bipyramid structure 17 is 0.78 eV above the lowest-energy species 14. In 17, five Nb–Nb bonds can be envisaged. For comparison, optimized structures of stable isomers 18–24 of $(\text{NbCo})_4$ are displayed in Fig. 3. As

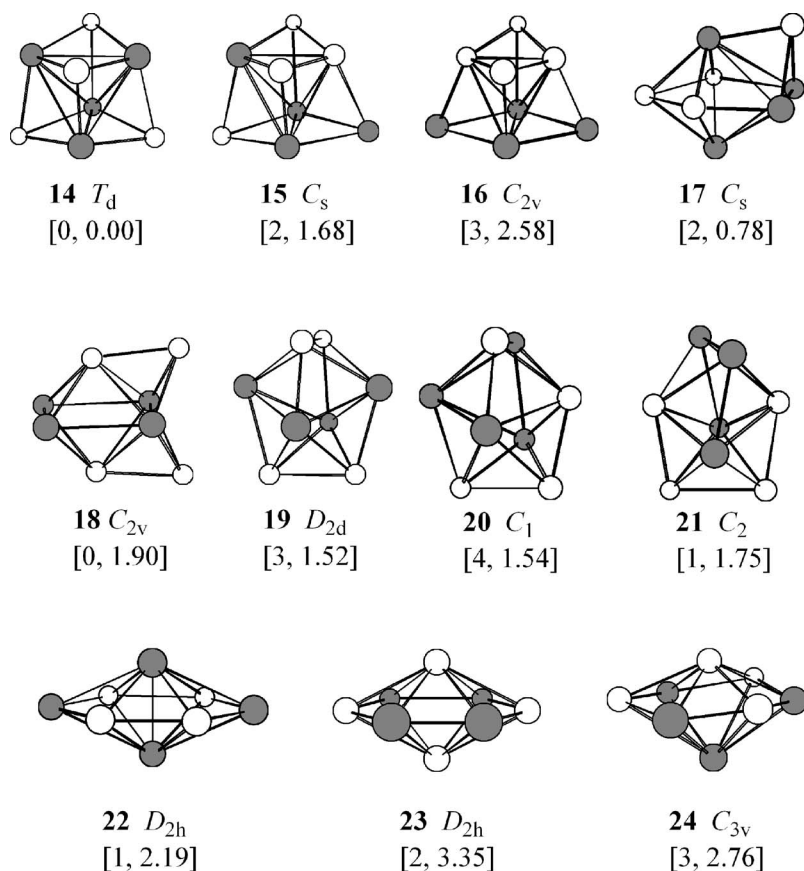


FIG. 3. Optimized geometries of $(\text{NbCo})_4$ clusters are shown with their spin (S) and relative energies (ΔE in eV), $[S, \Delta E]$, where the dark circle and empty circle correspond to Nb and Co atoms, respectively.

Fig. 3 shows, the stability of the binary $(\text{NbCo})_4$ cluster strongly depends on the atomic arrangement. The more Nb–Nb bonds in the Nb/Co cluster, the more stable the structure.

4. $(\text{NbCo})_5$

The $(\text{NbCo})_5$ cluster has quite rich structural varieties. Figure 4 displays the optimized structures of its possible stable isomers with different symmetries and spin states. At the relativistic DFT level, a capped octahedral structure 25 in C_{4v} symmetry ($S=3$) was found to be the ground state of the $(\text{NbCo})_5$ cluster. In the lowest-energy isomer, five niobium atoms form a tetragonal pyramid core Nb_5 and five cobalt atoms were bound to its five facets. Nb–Nb separations in 25 vary from 2.83 to 2.98 Å and Nb–Co bond lengths are in the range from 2.28 to 2.55 Å. Calculations reveal that the spin states of $S=1$ and 2 with the same structure as 25 are slightly higher in energy than the most stable septet state (25) by less than 0.16 eV. The next stable species 26 is 0.57 eV above 25, in which five cobalt atoms are in the same side of the Nb_5 core. PW91 optimized structures of other metastable isomers

27–45 are displayed in Fig. 4. Like the $(\text{NbCo})_4$ cluster, the more the short Nb–Nb bonds, the more stable the structure.

In general, the $(\text{NbCo})_n$ ($2 \leq n \leq 5$) clusters prefer a 3D structure, although linear and planar conformations are local minima on the potential-energy surfaces. Similar to the molecular skeleton of boranes,⁴⁰ clusters with high stability have compact structures with more strong metal-metal bonds. In the most stable tautomers, Nb atoms form a core with high symmetry and Co atoms are capped to the facets of the Nb_n core. Such building feature in clustering of the Nb/Co system is related to the relative strength of the metal-metal bond: $\text{Nb–Nb} > \text{Nb–Co} > \text{Co–Co}$. The presence of a symmetric core results in the most stable structures to have high symmetries such as C_{3v} for $(\text{NbCo})_3$, T_d for $(\text{NbCo})_4$, and C_{4v} for $(\text{NbCo})_5$.

B. Bond properties

Table II presents bond lengths and Mulliken overlap populations (MOPs) of selected low-energy species in the Nb/Co systems. Data in Table II show that, in general, Nb–Nb bond lengths are longer than Nb–Co and Co–Co

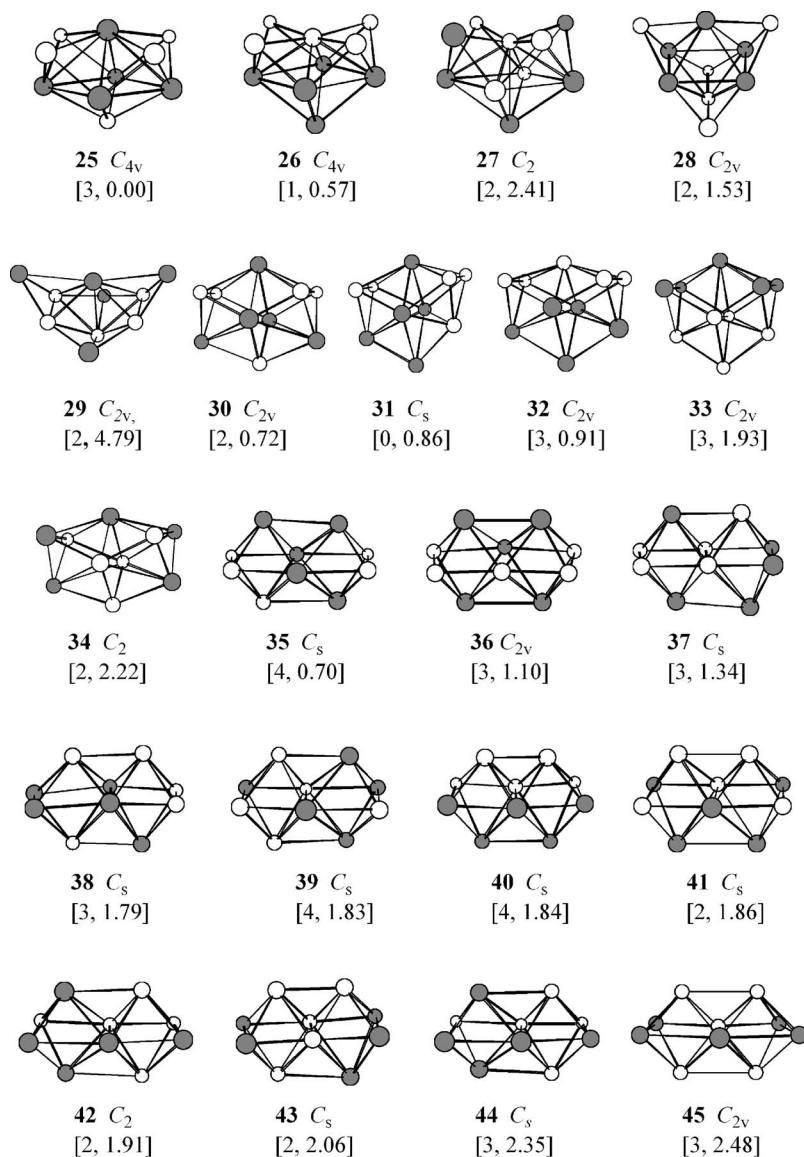


FIG. 4. Optimized geometries of $(\text{NbCo})_5$ clusters are shown with their spin (S) and relative energies (ΔE in eV), $[S, \Delta E]$, where the dark circle and empty circle correspond to Nb and Co atoms, respectively.

bonds, because the niobium atom radius (1.63 Å) is larger than that of cobalt (1.25 Å). In the clusters $(\text{NbCo})_n$, the inner core of the clusters has long metal-metal bonds due to the traction of the outer atoms; while the inner-outer shell separations are small to maintain minimal surface energy. For instance, in the lowest-energy structures of $(\text{NbCo})_3$ and $(\text{NbCo})_4$, 8 and 14, the Nb–Nb bond lengths in the moieties of Nb_3 and Nb_4 are 2.56 and 2.84 Å, respectively, notably longer than the average bond lengths of 2.39 and 2.54 Å in bare clusters Nb_3 and Nb_4 .²¹ Such remarkable bond length increment indicates that relatively strong Nb–Nb bonds are weakened by the inner-outer shell Nb–Co interactions. Bond lengths and bonding populations in Table II reveal that multiple Nb–Nb bonds may have been formed in the small cluster $(\text{NbCo})_2$.

The lowest-energy structure 14 of $(\text{NbCo})_4$ is quite an interesting cluster for its unique high stability and symmetry. Previous studies^{35,41} point out that the ground state of Nb_4 is a regular tetrahedron in T_d symmetry, and its ten bonding orbitals are full occupied by valence electrons. Our previous computational analyses indicate that these ten orbitals are divided into two types according to their bonding characters. Orbitals a_1+e+t_2 constitute the tetrahedral skeleton, and other bonding orbitals a_1+t_2 locate in trigonal facets.⁴² To match these orbitals of the Nb_4 core, four capped Co atoms also keep T_d symmetry. A linear combination of valence orbitals of Nb_4 and four Co atoms gives rise to a complex orbital pattern in 14, as shown in Fig. 5. The lowest-energy state (14) has an electron configuration:

$$(1a_1)^2(1t_2)^6(2a_1)^2(1e)^4(2t_2)^6(2e)^4(1t_1)^6(3t_2)^6(4t_2)^6 \\ \times (2t_1)^6(3a_1)^2(5t_2)^6.$$

All occupied valence orbitals, except $3a_1$, $4t_2$, and $2t_1$, have a character of strong Nb–Co bonding and they are bonding molecular orbitals (BMOs). The $3a_1$ comes from the anti-symmetric overlap of $1a_1$ (Nb_4) and $1a_1$ (4Co). The orbitals $4t_2$ and $2t_1$ are the nonbonding molecular orbitals (NBMOs) contributed by Co atoms. The closed-shell structure composed of BMOs in 14 accounts for its high stability. Note that the Co–Co separation in the lowest-energy structure 14 is 3.63 Å and there are no virtual Co–Co bonding interactions.

Furthermore, we calculated its nucleus-independent chemical shift⁴³ (NICS) by the GIAO-PW91/Lan12DZ method^{44–47} implemented by the GAUSSIAN98 package.⁴⁸ The value of the NICS at the central position of the lowest-energy structure 14 is -97.13 ppm, which indicates that 14 has spherical aromaticity similar to other aromatic deltahedral clusters^{49,50} (the negative NICS value, aromaticity; the positive NICS value, antiaromaticity⁴⁷). The aromaticity, i.e., electron delocalization, will stabilize the cluster. We extended such calculations to a capped octahedral anion $\text{Nb}_6\text{Co}_4^{2-}$ whose geometry is analogous to isomer 28 and four Co atoms are capped on the octahedral core Nb_6 ($R_{\text{Nb-Nb}} = 2.76$ Å and $R_{\text{Nb-Co}} = 2.41$ Å). Like 14, $\text{Nb}_6\text{Co}_4^{2-}$ in T_d symmetry has high stability and its average binding energy per atom is 4.02 eV. In $\text{Nb}_6\text{Co}_4^{2-}$, all bonding MOs have been occupied (68 valence electrons occupy four a_1 , three e , two

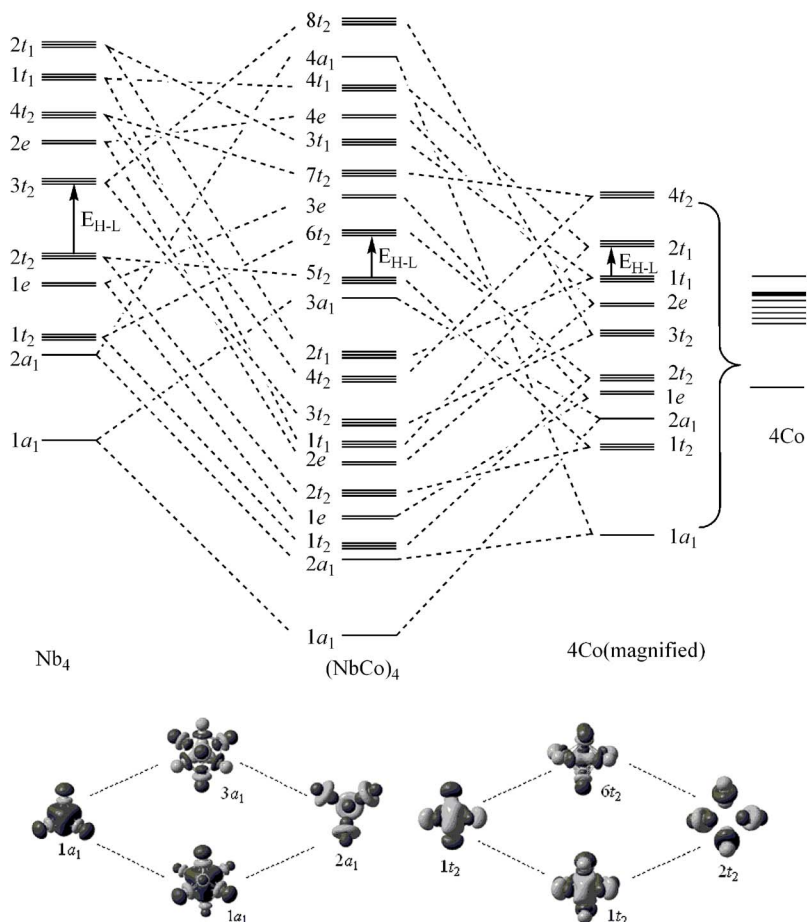


FIG. 5. Molecular-orbital correlation diagram of $(\text{NbCo})_4$ in the ground state and its components of Nb_4 and 4Co and selected molecular orbitals are depicted.

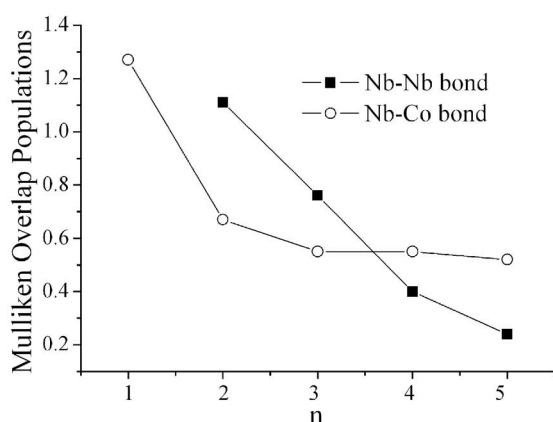
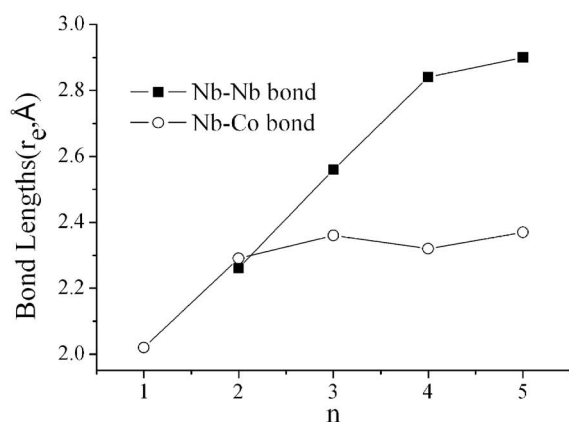


FIG. 6. A comparison of the bond lengths and Mulliken overlap populations vs the size of the cluster for Nb–Nb and Nb–Co bonds of $(\text{NbCo})_n$ ($n \leq 5$) in their ground states.

t_1 , and six t_2 orbitals) and such electronic shell closure will stabilize the cluster anion. The predicted NICS at the central position is 18.19 ppm, indicating that this cluster has an antiaromaticity and its valence electrons are less delocalized than 14.

The size dependence of the bond lengths and MOPs for Nb–Nb and Nb–Co bonds are depicted in Fig. 6. As Fig. 6 displays that the Nb–Nb bond length has a sharp increase (from 2.26 to 2.90 Å) as the cluster increases from $n=2$ to 4, but this change starts to become smoothly from $n \geq 4$. On the contrary, the Nb–Co bond maintains in the range of 2.2–2.4 Å when $n \geq 2$. The corresponding MOP changes of Nb–Nb and Nb–Co bonds have a similar tendency, and the former decreases strikingly as the size of the cluster increases and the latter keeps about 0.5 as $n \geq 2$. As the MOPs show in Fig. 6 and Table II, the Nb–Co bond may become stronger than the Nb–Nb bond as the size of the binary cluster increases.

Mulliken charges in Table II show that the charge transfer from Nb to Co in the binary clusters is universal, i.e., in the metal-metal bonding between Nb and Co atoms, Nb behaves as a donor while Co behaves as an acceptor. This can be ascribed to relatively higher electronegativity of Co than that of Nb.⁵¹ Besides niobium-cobalt bimetallic clusters,

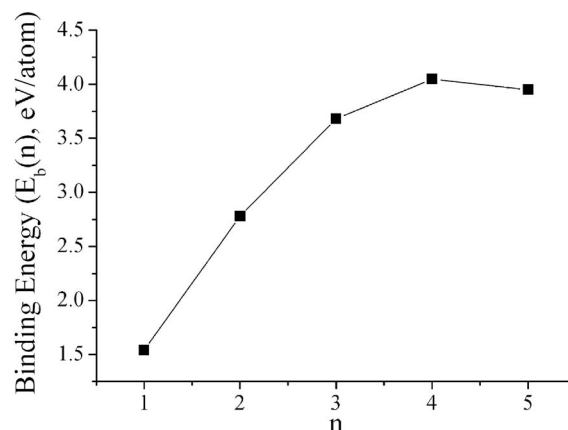


FIG. 7. Size dependence of the binding energies per atom of $(\text{NbCo})_n$ ($n \leq 5$) in their ground states.

other binary clusters composed of early- and late-transition metals, such as Ti–Ni, have similar bonding features.⁵²

C. Binding energy

For comparison of the relative stabilities of the $(\text{NbCo})_n$ clusters, the average binding energy per atom was calculated. The binding energy $E_b(n)$ was defined as

$$E_b(n) = [nE_t(\text{Nb}) + nE_t(\text{Co}) - E_t(\text{NbCo})_n]/2n,$$

where E_t is the total energy of the respective atoms or clusters. A spin-polarized $4d^4s^1(s^1d_{xy}^1d_{zx}^1d_{zy}^1d_{x^2-y^2}^1d_{z^2}^0)$ configuration of niobium and a $3d^84s^1(s^1d_{xy}^1d_{zx}^2d_{zy}^2d_{x^2-y^2}^2d_{z^2}^1)$ configuration of cobalt were used for the atomic reference energies, respectively. Table II presents the binding energies per atom for selected low-energy isomers. Note that the binding energies are densely distributed within a narrow range from 3.6 to 4.0 eV when $n \geq 3$. As Fig. 7 displays, the binding energy notably increases as the cluster size increases up to $n=4$, then it maintains at about 3.9 eV. Due to the presence of a large portion of surface atoms, the binding energy is smaller

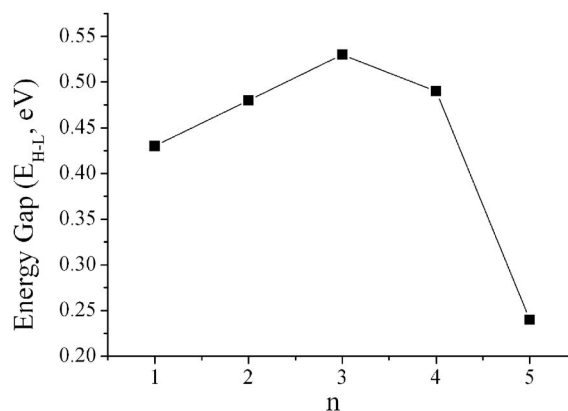


FIG. 8. Size dependence of the energy gaps of $(\text{NbCo})_n$ ($n \leq 5$) in their ground states.

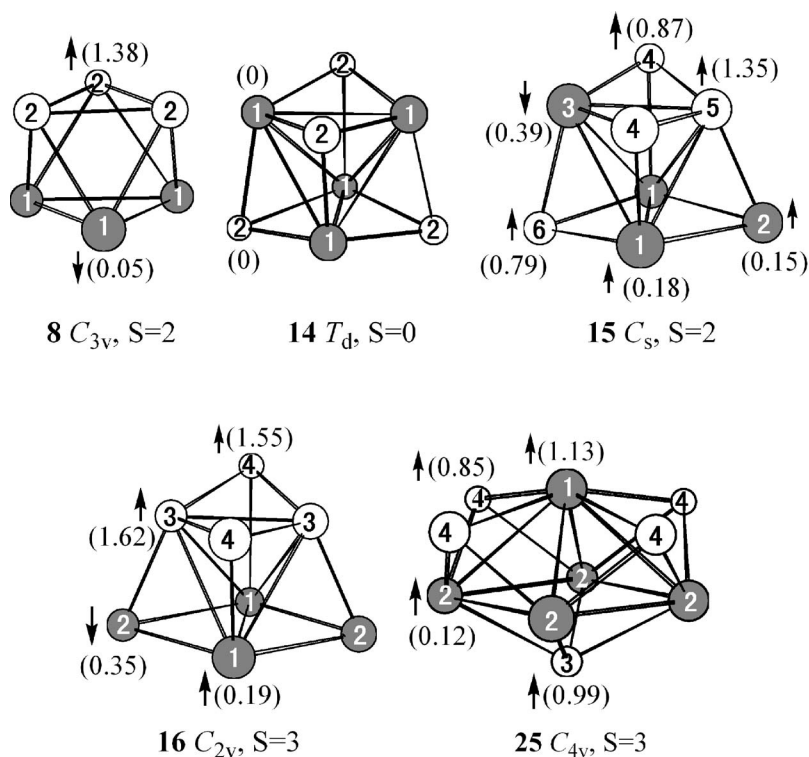


FIG. 9. The local magnetic moments per atom of 8, 14, and 25 in their ground states, as well as the other two low-lying states 15 and 16, where atoms with the same magnetic moments are indicated by the same number in circles. The arrows \uparrow and \downarrow indicate the direction of spin polarization at each site and the corresponding magnetic moments (in μ_B) are given within the parentheses at each site. The molecular symmetry and the spin numbers S are also displayed.

than that of the bulk alloy [in bulk, $E_b^{\text{exp}}(\text{Nb})=8.0$ eV and $E_b^{\text{exp}}(\text{Co})=4.55$ eV (Ref. 53)].

As Table II shows, a large highest occupied molecular orbital-lowest unoccupied molecular orbital (HOMO-LUMO) gap corresponds to a large binding energy for different isomers of the same cluster. However, with the increase of the cluster size the gap goes up first and then decreases, as shown in Fig. 8. A significant reduction of the energy gap appears in $(\text{NbCo})_5$ due to the involvement of more metal atoms in the metal-metal bonding.

D. Magnetic properties

It is now well characterized that, both experimentally¹⁷⁻¹⁹ and theoretically,^{5,16} the magnetic moment and magnetic anisotropy energy per atom are enhanced in small metallic clusters in comparison with the bulk metal. Previous studies have demonstrated that small Co_n clusters exhibit high magnetic moments of $\mu \approx 2.5\mu_B/\text{at.}$,⁵⁴ whereas Nb_n clusters are nonmagnetic. Table II presents the average spin densities of selected low-energy structures. Local magnetic moments per atom of selected structures 8, 14, 15, 16, and 25 have been shown in Fig. 9, where the numberings are used to distinguish the atoms with different magnetic moments.

As Fig. 9 shows, with the increase of Co atoms coordinated to Nb, the magnetic moment of Nb increases. For example, the Nb atom with the numbering 1 in 25 has a large magnetic moment of $1.13\mu_B$. On the contrary, the magnetic moments of Co atoms notably reduce with coordination of Nb to Co. When there are enough Nb atoms around the magnetic Co, the magnetic moment of cobalt disappears. This is in good agreement with the experiment.¹⁹ The overall average magnetic moments per atom will decrease gradually with

increase of the cluster size. The results of clusters 14–16 in Fig. 9 indicate that the magnitude of the atomic magnetic moment depends on the cluster structure as well as on the atomic arrangement. Furthermore, we notice that antiferromagnetic coupling pairs of Nb atoms exhibit in clusters 15 and 16. Such antiferromagnetic coupling is common for metals with roughly half-filled d band such as manganese clusters.⁵⁵

E. Vibrational spectra

Vibrational spectra could be structure probe because they are in general sensitive to the atomic configurations. We performed vibrational frequency calculations for all optimized structures. Figure 10 presents the calculated IR spectra of the lowest-energy structures. In particular, vibrational frequencies of $(\text{NbCo})_2$ in the ground state (1) range from 69 to 381 cm^{-1} . The highest peak corresponds to the bending mode of Nb–Co bonds in B_2 symmetry. For $(\text{NbCo})_3$ (8), vibrational frequencies vary from 122 to 342 cm^{-1} . The strongest absorption occurs at 259 cm^{-1} , which corresponds to a stretching mode of the Co/Nb layer. The $(\text{NbCo})_4$ cluster has a ground state 1A_1 in T_d symmetry and the strongest band occurs at 145 cm^{-1} , which has T_2 symmetry. For the $(\text{NbCo})_5$ cluster (25), it has more complex vibrational modes, and most of them involve coupled vibrational modes of the core and capped atoms. Vibrational frequencies range from 52 to 312 cm^{-1} , in which the strongest IR band lies at 129 cm^{-1} . Such predicted vibrational frequencies may be used for further exploration of these metal clusters in combination with spectroscopic experiments.

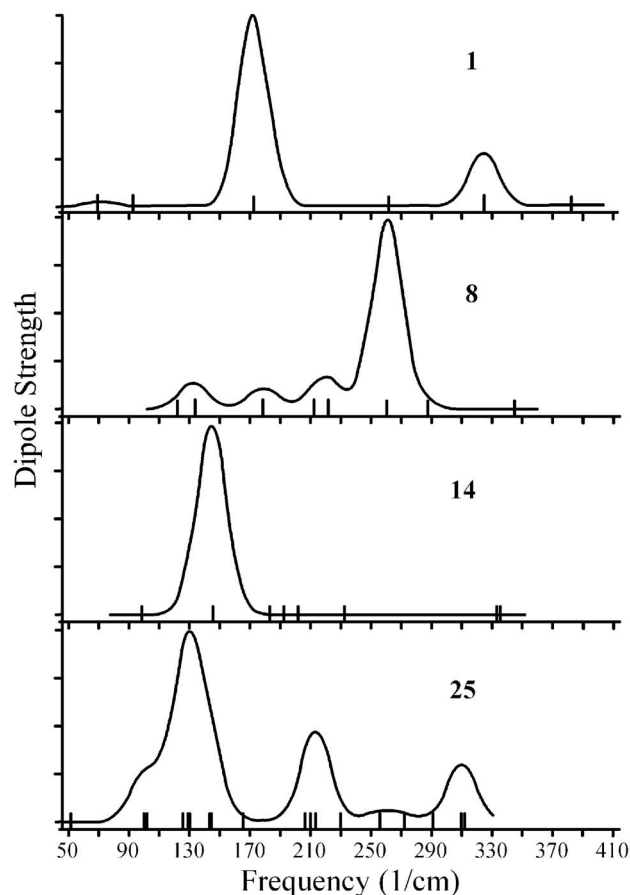


FIG. 10. Predicated vibrational spectra of $(\text{NbCo})_n$ ($2 \leq n \leq 5$) in their ground states. The small arrows on the base line indicate the peak positions of vibrational frequencies.

IV. CONCLUSIONS

Stable isomers of binary TM clusters $(\text{NbCo})_n$ ($n \leq 5$) have been investigated by a relativistic density-functional approach with the generalized gradient approximation available in the Amsterdam density functional program. The structures and stabilities of such clusters have been discussed on the basis of their binding energies and electronic structures. Metal-metal bonding interactions, magnetic properties, and vibrational spectra also have been analyzed in detail. Based on the present calculations, the following conclusions have been inferred:

- (i) Optimized geometries and energetics suggest that the binary Nb/Co clusters have a rich structural variety on the PES. The most stable clusters prefer to be a 3D compact structure with more strong metal-metal bonds. In the Nb/Co system, the strength of the metal-metal bond for small clusters follows the order: $\text{Nb-Nb} > \text{Nb-Co} > \text{Co-Co}$, whereas the Nb-Co bond may become stronger than the Nb-Nb bond with an increase of the size of the binary cluster.
- (ii) The ground states of $(\text{CoNb})_n$ clusters have a core composed of Nb atoms, and the symmetric Nb_n core results in the lowest-energy structure to have high symmetry for the $(\text{CoNb})_n$ clusters.
- (iii) Intermetallic bond significantly changes the electronic

structure of individual atoms. The charge transfer from Nb to Co is universal in these binary clusters, which leads to negatively charged cobalt atoms and positively charged niobium atoms.

- (iv) The presence of magnetic Co atoms around Nb increases the local magnetic moments of Nb while coordination of Nb atoms to Co may quench the magnetism of Co.

ACKNOWLEDGMENTS

This work has been supported by National Natural Science Foundation of China (Grant Nos. 90206038, 20373053, 20473062, 20233020, 20021002), Natural Science Foundation of Fujian Province (Grant No. 2002F010), and the Ministry of Science and Technology (Grant No. 2004CB719902).

- ¹ *Cluster Reactions*, edited by M. A. Duncan (Jai, Greenwich, CT, 1994).
- ² *Cluster Materials*, edited by M. A. Duncan (Jai, Greenwich, CT, 1998).
- ³ J. S. Alonso, *Chem. Rev.* (Washington, D.C.) **100**, 637 (2000).
- ⁴ J. R. Lombardi and B. Davis, *Chem. Rev.* (Washington, D.C.) **102**, 2431 (2002).
- ⁵ H. Q. Sun, Y. Ren, and G. H. Wang, *Phys. Status Solidi B* **225**, 301 (2001).
- ⁶ I. Efremenko and M. Sheintuch, *Chem. Phys. Lett.* **401**, 232 (2005).
- ⁷ W. J. C. Menezes and M. B. Knickelbein, *Chem. Phys. Lett.* **183**, 357 (1991).
- ⁸ R. D. Adams and B. Captain, *J. Organomet. Chem.* **689**, 4521 (2004).
- ⁹ M. A. Addicoat, M. A. Buntine, and G. F. Metha, *Aust. J. Chem.* **57**, 1197 (2004).
- ¹⁰ A. Nakajima, T. Kishi, T. Sugioka, Y. Sone, and K. Kaya, *J. Phys. Chem.* **95**, 6833 (1991); S. Nonose, Y. Sone, K. Onodera, S. Sudo, and K. Kaya, *ibid.* **94**, 2744 (1990).
- ¹¹ K. Hoshino, T. Naganuma, K. Watanabe, Y. Konishi, A. Nakajima, and K. Kaya, *Chem. Phys. Lett.* **239**, 369 (1995).
- ¹² A. Prammann, K. Koyasu, A. Nakajima, and K. Kaya, *J. Phys. Chem.* **106**, 2483 (2002); A. Prammann, A. Nakajima, and K. Kaya, *J. Chem. Phys.* **115**, 5404 (2001).
- ¹³ J. L. Yang, C. Y. Xiao, S. D. Xia, and K. L. Wang, *Phys. Rev. B* **48**, 12155 (1993).
- ¹⁴ D. Zitoun, M. Respaud, M. C. Fromen, and M. J. Casanove, *Phys. Rev. Lett.* **89**, 037203 (2002).
- ¹⁵ Š. Pick and H. Dreyssé, *J. Magn. Magn. Mater.* **240**, 337 (2002).
- ¹⁶ S. Dennler, J. Morillo, and G. M. Pastor, *J. Phys.: Condens. Matter* **16**, S2263 (2004).
- ¹⁷ M. Jamet, V. Dupuis, P. Mélinon, G. Guiraud, A. Pérez, W. Wernsdorfer, A. Traverse, and B. Bagueard, *Phys. Rev. B* **62**, 493 (2000).
- ¹⁸ V. Dupuis, M. Jamet, L. Favre, J. Tuillon-Combes, P. Melinon, and A. Perez, *J. Vac. Sci. Technol. A* **21**, 1519 (2003).
- ¹⁹ Š. Pick, I. Turek, and H. Dreyssé, *Solid State Commun.* **124**, 21 (2002).
- ²⁰ V. Kumar and Y. Kawazoe, *Phys. Rev. B* **65**, 125403 (2002).
- ²¹ J. E. Fowler, A. García, and J. M. Ugalde, *Phys. Rev. A* **60**, 3058 (1999).
- ²² H. Grönbeck and A. Rosén, *Phys. Rev. B* **54**, 1549 (1996); S. K. Nayak, B. K. Rao, S. N. Khanna, and P. Jena, *Chem. Phys. Lett.* **259**, 588 (1996).
- ²³ S. R. Liu, H. J. Zhai, and L. S. Wang, *Phys. Rev. B* **64**, 153402 (2001); R. Guirado-López, F. Aguilera-Granja, and J. M. Montejano-Carrizales, *ibid.* **65**, 045420 (2002).
- ²⁴ P. Mlynarski, M. Iglesias, M. Pereiro, D. Baldomir, and L. Wojtczak, *Vacuum* **54**, 143 (1999).
- ²⁵ C. Jamorski, A. Martinez, and M. Castro, *Phys. Rev. B* **55**, 10905 (1997).
- ²⁶ X. Wang, M. H. Lin, and Q. E. Zhang, *Acta Chim. Sinica* **62**, 1689 (2004).
- ²⁷ G. Te Velde and E. J. Baerends, *J. Comput. Phys.* **99**, 84 (1992).
- ²⁸ J. P. Perdew, J. A. Chevary, S. H. Vosko, K. A. Jackson, M. R. Pederson, D. J. Singh, and C. Fiolhais, *Phys. Rev. B* **46**, 6671 (1992).
- ²⁹ E. Van Lenthee, E. J. Baerends, and J. G. Snijders, *J. Chem. Phys.* **101**, 9783 (1994).
- ³⁰ E. Van Lenthee, J. G. Snijders, and E. J. Baerends, *J. Chem. Phys.* **105**, 6505 (1996).

- ³¹ A. M. James, P. Kowalczyk, R. Fournier, and B. Simard, *J. Chem. Phys.* **99**, 8504 (1993).
- ³² S. K. Loh, L. Lian, and P. B. Armentrout, *J. Am. Chem. Soc.* **111**, 3167 (1989).
- ³³ A. M. James, P. Kowalczyk, E. Langlois, M. D. Campbell, A. Ogawa, and B. Simard, *J. Chem. Phys.* **101**, 4485 (1994).
- ³⁴ K. Sohn, S. Lee, L. M. Bylander, and L. Kleinman, *Phys. Rev. B* **39**, 9983 (1989).
- ³⁵ L. Goodwin and D. R. Salahub, *Phys. Rev. A* **47**, R774 (1993).
- ³⁶ H. J. Fan, C. W. Liu, and M. S. Liao, *Chem. Phys. Lett.* **273**, 353 (1997).
- ³⁷ A. Kant and B. Strauss, *J. Chem. Phys.* **41**, 3806 (1964).
- ³⁸ J. G. Dong, Z. Hu, R. Craig, J. R. Lombardi, and D. M. Lindsay, *J. Chem. Phys.* **101**, 9280 (1994).
- ³⁹ C. A. Arrington, T. Blume, M. D. Morse, M. Doverstål, and U. Sassenberg, *J. Phys. Chem.* **98**, 1398 (1994).
- ⁴⁰ K. Wade, *Adv. Inorg. Chem. Radiochem.* **18**, 1 (1976).
- ⁴¹ D. Majumdar and K. Balasubramanian, *J. Chem. Phys.* **121**, 4014 (2004).
- ⁴² X. Wang, M. H. Lin, K. Tan, F. Wang, and Q. E. Zhang, *Chem. J. Chinese Univ.* (in press).
- ⁴³ P. v. R. Schleyer, C. Maerker, A. Dransfeld, H. Jiao, and N. J. R. v. E. Hommes, *J. Am. Chem. Soc.* **118**, 6317 (1996).
- ⁴⁴ K. Wolinski, J. F. Hilton, and P. Pulay, *J. Am. Chem. Soc.* **112**, 8251 (1990).
- ⁴⁵ D. Ditchfiels, *Mol. Phys.* **27**, 789 (1974).
- ⁴⁶ R. McWeeny, *Phys. Rev.* **126**, 1028 (1962).
- ⁴⁷ J. L. Dodds, R. McWeeny, and A. J. Sadlej, *Mol. Phys.* **34**, 1779 (1977).
- ⁴⁸ M. J. Frisch, G. W. Trucks, H. B. Schlegel *et al.*, GAUSSIAN98, revision A.9, Gaussian, Inc., Pittsburgh, PA, 1998.
- ⁴⁹ Z. Chen, A. Hirsch, S. Nagase, W. Thiel, and P. v. R. Schleyer, *J. Am. Chem. Soc.* **125**, 15507 (2003).
- ⁵⁰ R. B. King, Z. Chen, and P. v. R. Schleyer, *Inorg. Chem.* **43**, 4564 (2004).
- ⁵¹ *The Nature of The Chemical Bond and the Structure of Molecules and Crystals*, edited by L. Pauling (Cornell University Press, Ithaca, 1960).
- ⁵² K. Tan, Y. B. Gu, and M. H. Lin, *Chem. Res. Chin. Univ.* **21**, 96 (2005).
- ⁵³ *Metal Physics*, edited by D. Feng (Science, Beijing, 2000), Vol. 1, p. 22.
- ⁵⁴ J. L. Rodriguez-López, F. Aguilera-Granja, K. Michaelian, and A. Vega, *Phys. Rev. B* **67**, 174413 (2003).
- ⁵⁵ N. O. Jones, S. N. Khanna, T. Baruah, and M. R. Pederson, *Phys. Rev. B* **70**, 045416 (2004).